




Rare Finding of a 100 Kpc Large, Double-lobed Radio Galaxy Hosted in the Narrow-line Seyfert 1 Galaxy SDSS J103024.95+551622.7

Suvendu Rakshit^{1,2} , C. S. Stalin², Ananda Hota³, and Chiranjib Konar⁴¹ Astronomy Program, Department of Physics and Astronomy, Seoul National University, Seoul 151-742, Republic of Korea; suvenduat@gmail.com² Indian Institute of Astrophysics, Block II, Koramangala, Bangalore-560034, India³ UM-DAE Centre for Excellence in Basic Sciences, Vidyanageri, Mumbai 400098, India⁴ Amity Institute of Applied Sciences, Amity University Uttar Pradesh, Sector-125, NOIDA, U.P., India

Received 2018 April 10; revised 2018 November 5; accepted 2018 November 5; published 2018 December 26

Abstract

Among the many varieties of active galactic nuclei (AGNs) known, narrow-line Seyfert 1 (NLSy1) galaxies are a puzzling class, particularly after the discovery of γ -ray emission in a handful of them using observations from the *Fermi* Gamma-ray Space Telescope. Here, we report the discovery of a rare, large, double-lobed radio source with its radio core associated with an NLSy1 galaxy, SDSS J103024.95+551622.7, at $z = 0.435$. The lobe separation is 116 kpc which is the second largest known projected size among NLSy1 radio sources. This finding is based on the analysis of 1.4 GHz data from the Faint Images of the Radio Sky at Twenty-centimeters archives. Along with the core and edge-brightened lobes we detected a significant (30%) fraction of clear diffuse emission showing typical back-flow from FR II radio galaxy lobes. For the source, we estimated a jet power of 3×10^{44} erg s⁻¹, suggesting that its jet power is similar to that of classical radio galaxies. Emission from the source is also found to be non-variable both in the optical and mid-infrared bands. Identification of more such sources may help to reveal new modes of AGNs and to understand their role in black hole galaxy evolution.

Key words: galaxies: active – galaxies: individual (SDSS J103024.95+551622.7) – galaxies: Seyfert

1. Introduction

Narrow-line Seyfert 1 (NLSy1) galaxies are a peculiar type of active galactic nuclei (AGNs), characterized by narrow H β emission line with full width at half maximum (FWHM) less than 2000 km s⁻¹ and weak [O III] lines relative to H β with [O III]/H β < 3 (Osterbrock & Pogge 1985; Goodrich 1989). In addition, these sources have strong Fe II emission in the UV optical region of the spectrum, soft X-ray excess, steep soft X-ray spectrum (Boller et al. 1996; Wang et al. 1996), and show rapid large-amplitude X-ray flux variations (Boller et al. 1996; Leighly 1999; Rani et al. 2017). These extreme properties shown by NLSy1 galaxies are generally attributed to them having low-mass black holes (BHs) and accreting close to the Eddington limit (Boroson & Green 1992; Sulentic et al. 2000). However, recent results on a limited number of sources indicate that NLSy1 galaxies also have BH masses similar to broad-line Seyfert 1 (BLSy1) galaxies and their observed BH mass deficit could be due to geometrical effects (Calderone et al. 2013; Baldi et al. 2016; Liu et al. 2016; Rakshit & Stalin 2017).

A fraction of about 7% NLSy1 galaxies are known to be radio-loud, characterized by the radio-loudness parameter $R^5 > 10$ (Kellermann et al. 1989). About 2% of NLSy1 galaxies are found to be very radio-loud (see Komossa et al. 2006; Zhou et al. 2006). Increasing the sample of NLSy1 galaxies yields a low fraction of radio-loud NLSy1 (RL-NLSy1) galaxies of around 5% (Rakshit et al. 2017). The low fraction of RL-NLSy1 galaxies relative to the quasar population of AGNs indicates that they are either a rare population of sources or they are weak jet sources. However, detection of strong radio emission, compact cores with high brightness temperature, significant radio variability, etc., in some NLSy1

galaxies indicate the presence of relativistic jets with blazar-like characteristic (Yuan et al. 2008; Lähteenmäki et al. 2017). Some NLSy1 galaxies exhibit flat or inverted radio spectra while others show steep radio spectra (Gu et al. 2015). Interestingly, from about a dozen RL-NLSy1 galaxies, γ -ray emission has been detected by the Large Area Telescope (e.g., Abdo et al. 2009; D’Ammando et al. 2015; Paliya et al. 2018) on board the *Fermi* Gamma-ray Space Telescope, making them very special candidates to study the jet formation process. The broadband spectral energy distributions (SEDs) of these γ -ray-detected NLSy1 galaxies have the double-hump structure typical of blazars and specifically show a resemblance to the flat spectrum category of AGNs (Paliya et al. 2018). Accordingly, the low-energy humps of their SEDs are explained by synchrotron emission processes and their high-energy humps are attributed to external Compton processes.

In terms of radio morphology, RL-NLSy1 galaxies are generally considered to be compact and unresolved at the resolution of the images available in the Faint Images of the Radio Sky at Twenty-centimeters (FIRST) archives based on observations with the Very Large Array in its B configuration. Only recently, RL-NLSy1 galaxies are known to have kiloparsec-scale radio emission and to date less than two dozen NLSy1 galaxies have been detected with kpc scale jets (Whalen et al. 2006; Antón et al. 2008; Gliozzi et al. 2010; Doi et al. 2012, 2015; Richards & Lister 2015; Congiu et al. 2017), with linear sizes lesser than 150 kpc. As presented in Table 1, we see that none of them show FR II (Fanaroff & Riley 1974) double-lobed structure at 100 kpc scales, comparable to standard radio galaxies (Kapahi 1989; Singal 1993). Detection of 100 kpc scale emissions in RL-NLSy1 galaxies is extremely important as this can shed new light on the jet-launching mechanism. Since radio jets are typically launched at low accretion rate onto high-mass spinning BHs hosted in ellipticals, finding them in NLSy1 galaxies (typically low BH

⁵ R is defined as the ratio of flux density in the radio band at 5 GHz and that in the optical B -band.

Table 1
Details of Radio-loud NLSy1 Galaxies with Larger Than 20 kpc Scale Radio Structures

Name	R.A. (2000)	Decl. (2000)	z	FWHM (km s^{-1})	$\log(M_{\text{BH}}/M_{\odot})$	D_{proj} (kpc)	$\log P_{1.4}$ (erg s^{-1})	θ_{FIRST}	α	W1 (mag)	References
(1)	(2)	(3)	(4)	(5)	(6)	(7)	(8)	(9)	(10)	(11)	(12)
1H 0323+342*	03:24:41.1	+34:10:46	0.063	1520	7.3	48	40.91	1.21	0.1	10.74 ± 0.02	Doi et al. (2012)
PKS 0558-504	05:59:47.4	-50:26:52	0.137	1250	7.8	34	41.09	1.18	-0.3	10.67 ± 0.02	Gliozzi et al. (2010)
PMN J0948+0022*	09:48:57.3	+00:22:26	0.585	1432	7.5	104	42.30	1.01	0.77	13.28 ± 0.02	Doi et al. (2012)
NVSS J095317+283601	09:53:17.1	+28:36:02	0.659	2162	7.8	70.2	42.06	1.03	-0.50	14.80 ± 0.03	Richards & Lister (2015),
SDSS J103024.95+551622.7	10:30:24.9	+55:16:23	0.435	2170	7.9	116.0	41.47	1.69	-0.65	12.78 ± 0.02	This work
SDSS J110006.07+442144.3	11:00:06.1	+44:21:44	0.84	1900	7.0	150	41.82	1.37	0.20	17.40 ± 0.13	Tanaka et al. (2014), Gabányi et al. (2018)
SDSS J120014.08-004638.7	12:00:14.1	-00:46:39	0.179	1945	7.4	86	40.43	1.81	...	13.18 ± 0.02	Doi et al. (2012)
SDSS J122222.55+041315.7*	12:22:22.5	+04:13:16	0.966	1734	8.2	80	43.67	1.03	0.30	12.80 ± 0.02	Yao et al. (2015)
Mrk 783	13:02:58.8	+16:24:27	0.067	770	7.6	26.0	39.64	1.24	0.67	11.37 ± 0.02	Congiu et al. (2017)
NVSS J143509+313149	14:35:09.5	+31:31:48	0.502	1719	7.5	30.6	41.75	1.06	-0.72	14.39 ± 0.03	Richards & Lister (2015)
SDSS J145041.93+591936.9	14:50:41.9	+59:19:37	0.202	1159	6.5	38	39.74	1.02	...	13.23 ± 0.02	Doi et al. (2012)
PKS 1502+036*	15:05:06.5	+03:26:31	0.409	1082	6.6	<25	42.46	1.02	0.70	14.02 ± 0.02	D'Ammando et al. 2013
FBQS J1644+2619*	16:44:42.5	+26:19:13	0.144	1507	6.9	60	40.84	1.01	0.38	13.28 ± 0.02	Doi et al. (2012)
NVSS J172206+565452	17:22:06.0	+56:54:52	0.426	1385	7.4	22.8	41.53	1.03	-0.64	14.39 ± 0.03	Richards & Lister (2015)

Note. Those marked with * are sources that are emitters of γ -rays. The columns are (1) object name; (2) R.A.; (3) decl.; (4) redshift; (5) $H\beta$ line FWHM (km s^{-1}); (6) logarithmic black hole mass (M_{\odot}); (7) projected size of the radio structure (kpc); (8) logarithmic radio power at 1.4 GHz (erg s^{-1}); (9) θ_{FIRST} ; (10) radio spectral index; (11) *WISE* magnitude in *W1*-band ($2.4 \mu\text{m}$), and (12) references.

mass, with high accretion rate in disk galaxies with gas-rich central regions) is in clear contrast to expectations (Berton et al. 2018).

In this paper, we report the detection of 100 kpc radio emission with standard FR II radio galaxy-like lobes, from SDSS J103024.95+551622.7, which was recently classified as a NLSy1 galaxy by Rakshit et al. (2017) using Sloan Digital Sky Survey (SDSS) DR 12 spectroscopic data (Alam et al. 2015). This source has $\text{FWHM}(\text{H}\beta) = 2170 \pm 27 \text{ km s}^{-1}$, $F(\text{O III})/F(\text{H}\beta) = 0.2$, $R_{4570} = 0.15$, monochromatic luminosity at 5100 \AA , $\log \lambda L_{5100} = 45.13 \text{ (erg s}^{-1}\text{)}$, and a BH mass of $\log M_{\text{bh}}/M_{\odot} = 7.96$ (Rakshit et al. 2017). In the soft X-ray (0.1–2 KeV) using *ROSAT* observations, it was found to have a steep photon index of $\Gamma = -2.61 \pm 0.82$ (Boller et al. 2016). The paper is structured as follows. The sample and data are discussed in Section 2. The results are given in Section 3 followed by their interpretation and a discussion in Section 4. Conclusions are given in Section 5. A cosmology with $H_0 = 70 \text{ km s}^{-1} \text{ Mpc}^{-1}$, $\Omega_m = 0.3$, and $\Omega_{\lambda} = 0.7$ is used throughout.

2. Sample and Data

Our NLSy1 galaxy sample consists of all the 11,101 NLSy1 galaxies cataloged by Rakshit et al. (2017) from the SDSS DR 12 spectroscopic database. This is about a five-fold increase in the number of NLSy1 galaxies known prior to this work from Zhou et al. (2006). To find the radio counterparts to the NLSy1 galaxies reported in Rakshit et al. (2017), we cross-matched each NLSy1 galaxy with the FIRST catalog (Catalog version 14dec17⁶) around a circular region of radius 2 arcsec. This search provided us with a sample of 555 NLSy1 galaxies detected by FIRST. We then visually examined each of these 555 FIRST-detected NLSy1 galaxies for the presence of extended radio emission. This examination led to the discovery of one source, J103024.95+551622.7, with a very large extended radio emission. The radio core coincides with the optical nucleus with extended emission on both sides.

3. Results

We report the detection of a large kpc scale structure in an RL-NLSy1 galaxy based on the analysis of the FIRST images. It was discovered in the course of our analysis of the radio properties of the new sample of NLSy1 galaxies recently published by Rakshit et al. (2017). Figure 1 shows the radio contours of J103024.95+551622.7 from the FIRST image at 1.4 GHz superposed on its SDSS *r*-band image.

3.1. Radio Structure

The source has a radio core ($\alpha_{2000} = 10:30:24.787$, $\delta_{2000} = 55:16:18.48$ with peak flux = 14 mJy beam^{-1}) and extended radio structures. The angular separation between the northeast (NE) (72 mJy beam^{-1}) and southwest (SW) (21 mJy beam^{-1}) peaks is 20.5 arcsec which for the redshift of the host galaxy corresponds to a projected size⁷ of 116 kpc. Along with peaks at the lobes and the radio core coinciding with the host galaxy seen in the SDSS *r*-band image, there is significant diffuse emission present on either side of the double lobe. This is strong evidence that the NE and SW peaks are not unrelated

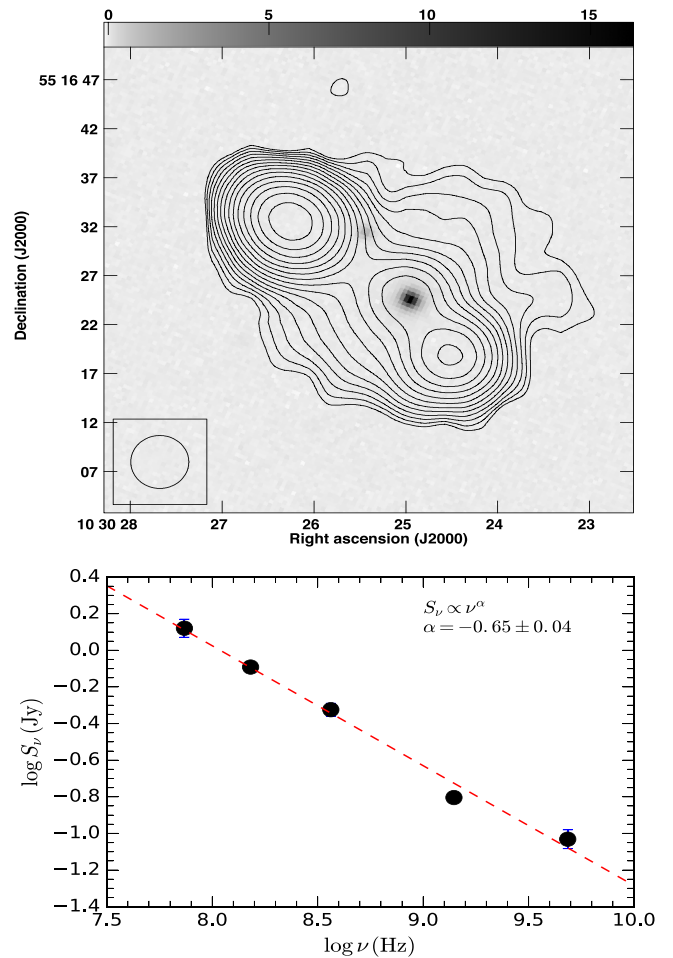


Figure 1. Top: radio contours from 1.4 GHz FIRST survey superposed on an SDSS *r*-band image in gray scale. Angular resolution and rms noise in the image are 5.4 arcsec and $0.15 \text{ mJy beam}^{-1}$ respectively. Contour levels are plotted as rms noise times $(-4, -2.82, 2.820, 4, 5.650)$ in steps of $\sqrt{2}$. Bottom: radio spectral energy distribution from non-simultaneous data. The best-fit line ($S_{\nu} \propto \nu^{\alpha}$ with a power-law index of $\alpha = -0.65 \pm 0.04$) is shown as a dashed line.

point sources but constitute a single radio galaxy with FR II-like radio structure with back-flow from hotspot regions causing the diffuse emission. Integrated flux calculated for the whole source from the FIRST image is 155 mJy. So the diffuse emission (subtracting the core and peaks at lobes from the integrated flux $(155 - (14 + 72 + 21)) = 48 \text{ mJy}$) constitutes the highest 30% of the whole radio source flux density. It may also be noted that the radio source (lobe–core–lobe) does not lie in a straight line and is slightly bent with the NE lobe brighter than the SW counterpart. Also, the presence of diffuse radio emission at the resolution of FIRST can be established from the dimensionless concentration parameter (Ivezić et al. 2002), $\theta_{\text{FIRST}} = \sqrt{S_{\text{int}}/S_{\text{peak}}}$, where S_{int} and S_{peak} are the integrated and peak flux densities of the source respectively. θ_{FIRST} is found to be 1.69, much larger than the value of 1.06 above which a source is defined as “resolved” by Kimball & Ivezić (2008), indicating extended emission. Since FIRST is a high-resolution survey, it is insensitive to the very extended emission originating from the lobes. However, the NRAO VLA Sky Survey (NVSS) at the same frequency provides low-resolution images, thus detecting much more extended emission. Therefore, following Singh et al. (2015),

⁶ <http://sundog.stsci.edu/first/catalogs.html>

⁷ Hereafter, all sizes are projected size unless specified otherwise.

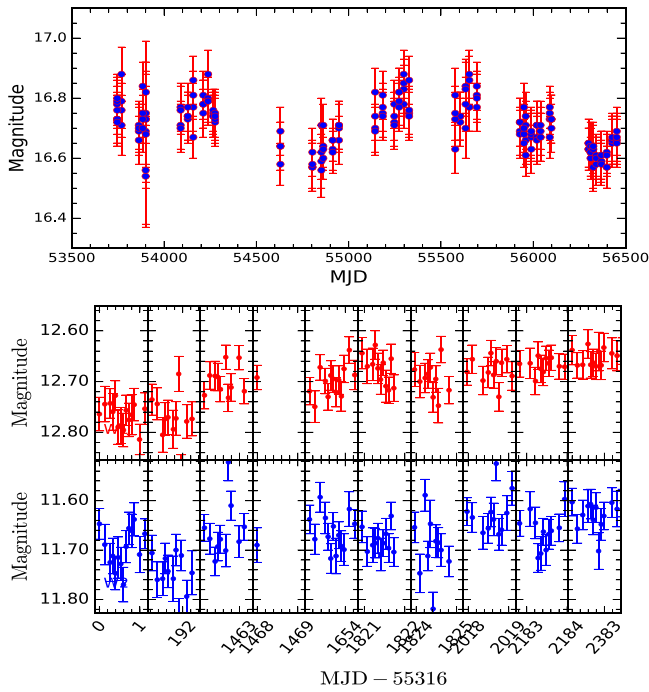


Figure 2. Top: optical V-band light curve of SDSS J103024.95+551622.7 obtained from the Catalina Real Time Transient Survey. Bottom: infrared 3.4 μm (upper) and 4.6 μm (lower) light curves.

we estimated $\theta_{\text{NVSS-FIRST}} = \sqrt{S_{\text{NVSS,int}}/S_{\text{FIRST,int}}}$, where $S_{\text{NVSS,int}}$ and $S_{\text{FIRST,int}}$ are the integrated flux densities obtained from NVSS and FIRST images respectively. The value of $\theta_{\text{NVSS-FIRST}}$ turns out to be 2.18, suggesting the presence of an additional faint low-surface-brightness radio component in the source apart from the extended radio emission detected in FIRST.

To estimate the radio spectral index (α) we collected multi-frequency radio data from the NASA/IPAC Extragalactic Database (NED)⁸ and estimated α using data from 74 MHz to 5 GHz utilizing a linear least-squares fit in the log-log plane. This is shown in the bottom panel of Figure 1. A steep radio spectrum ($S_\nu \propto \nu^\alpha$) with $\alpha = -0.65 \pm 0.04$ has been found for this object, suggesting extended emission originating from the young radio lobes.

3.2. Variability

The variability of the source in the optical and mid-IR bands was also investigated using data from the Catalina Real Time Transient Survey (CRTS; Drake et al. 2009) and the *Wide-field Infrared Survey Explorer* (WISE; Wright et al. 2010) database, respectively. The CRTS optical light curve is shown in the top panel of Figure 2. The amplitude of variability (σ_m) was calculated following Sesar et al. (2007) (see also Ai et al. 2010; Rakshit & Stalin 2017). The source is found to be non-variable in the optical. It is also found to be non-variable in the mid-IR W1 and W2 bands both on short (~ 1 day) and long timescales (~ 7 yr).

3.3. Optical Spectra

To check on the NLSy1 galaxy classification of SDSS J103024.95+551622.7, we collected the SDSS spectra,

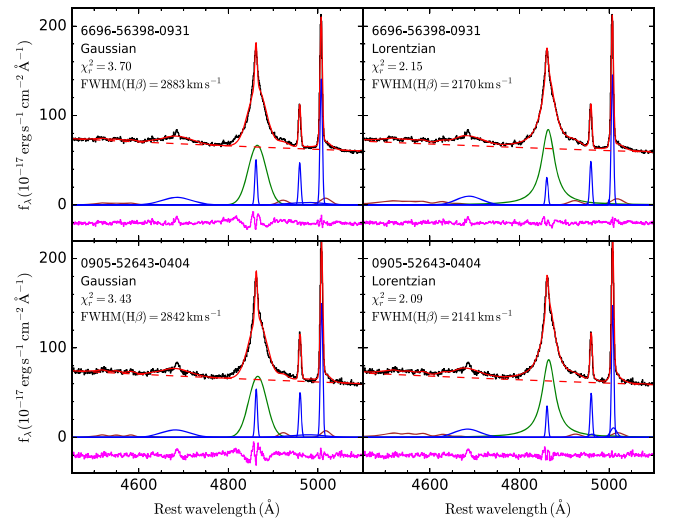


Figure 3. Spectral fittings of SDSS J103024.95+551622.7 around H β emission line regions for two different epochs shown in the upper and lower panel with labels indicating PLATE-MJD-FIBER of the SDSS. The broad emission line is fitted using a Gaussian (left) and a Lorentzian (right). The observed spectrum (black) and the overall fitted spectrum (red) are shown with the decomposed individual components; broad H β is in green, narrow H β , [O III] doublet and broad He II lines are in blue, and Fe II lines are in brown. The power-law continuum is shown as a red-dashed line. The residual is shown in magenta and the reduced- χ^2 of the fit is shown in each panel.

removed the effects of Galactic extinction, brought it to the rest frame, and re-analyzed it using the spectral decomposition procedure described by Rakshit et al. (2017) but without subtracting the host galaxy component, which is negligible as the redshift of the object is $z = 0.4347$. The source was observed twice, hence we fitted both the spectra as shown by the black line in the upper and lower panels of Figure 3 for two different cases: when the broad H β component was fitted using a Gaussian function (left) and a Lorentzian function (right). A Lorentzian function provides a better fit to the spectra, having lower reduced- χ^2 values in both spectra. The use of a Lorentzian function to fit the broad component of the H β emission naturally provides narrower FWHMs which are $2170 \pm 45 \text{ km s}^{-1}$ and $2140 \pm 38 \text{ km s}^{-1}$ for the two epochs compared to $2883 \pm 34 \text{ km s}^{-1}$ and $2842 \pm 70 \text{ km s}^{-1}$, respectively, found using a Gaussian function. The canonical definition of NLSy1 galaxies pertain to sources with $\text{FWHM}(\text{H}\beta) < 2000 \text{ km s}^{-1}$ (Goodrich 1989). However, the criterion of $\text{FWHM}(\text{H}\beta) < 2200 \text{ km s}^{-1}$ has been used in the initial catalog of NLSy1 galaxies by Zhou et al. (2006) and recently by Rakshit et al. (2017) since the distribution of the broad H β line width is smooth with no sharp cutoff between NLSy1 and BLSy1 galaxies. Moreover, a higher cutoff of $\text{FWHM}(\text{H}\beta) < 4000 \text{ km s}^{-1}$ based on the quasar main sequence (Sulentic et al. 2000), a luminosity-dependent cutoff value for the H β line width (Laor 2000; Véron-Cetty et al. 2001), or an Eddington ratio cutoff ($L/L_{\text{EDD}} \geq 0.25$) (Netzer & Trakhtenbrot 2007) have also been suggested for NLSy1 galaxies. The source studied here is close to the boundary of 2200 km s^{-1} adopted by Zhou et al. (2006) and Rakshit et al. (2017). However, it has a low [O III]/H β ratio and steep soft X-ray spectral index and an Eddington ratio of 1.01. Putting all the other characteristics together, it is most likely that SDSS J103024.95+551622.7 is an NLSy1 galaxy.

⁸ <http://nedwww.ipac.caltech.edu>

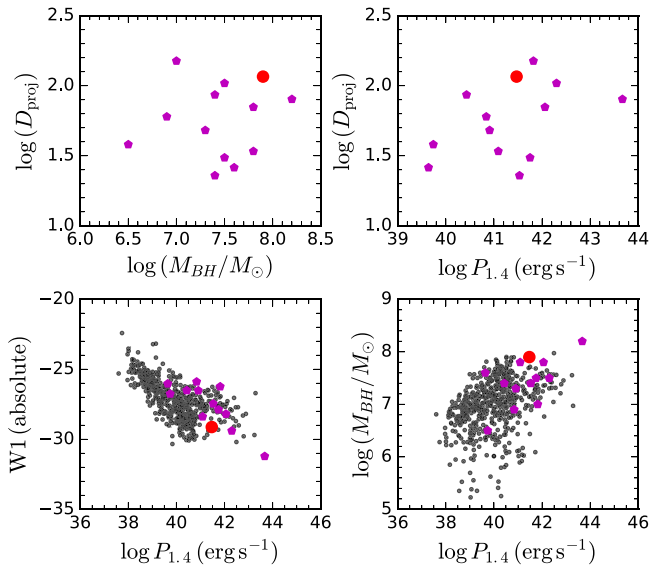


Figure 4. Projected size vs. black hole mass (upper left) and radio power at 1.4 GHz (upper right). *WISE* W1-band magnitude vs. radio power is shown lower left, and the black hole mass vs. radio power is shown lower right. The large red symbol represents SDSS J103024.95+551622.7. The polygons represent NLSy1 galaxies having larger than 20 kpc radio structure (see Table 1) except PKS 1502+036. The points in the lower panels represent NLSy1 galaxies detected in FIRST from Rakshit et al. (2017). In the lower left panel, only objects having signal-to-noise ratio >10 in *WISE* W1-band are plotted.

4. Interpretation and Discussion

4.1. Comparison with a Sample of NLSy1 Galaxies

We collected information on all NLSy1 galaxies having larger than 20 kpc radio emission from the literature and tabulate them in Table 1. Note that one of the sources, NVSS J095317+283601 in Table 1 has a FWHM of $H\beta$ ($2162 \pm 201 \text{ km s}^{-1}$) similar to that of SDSS J103024.95+551622.7. A higher FWHM ($H\beta$) will lead to a higher BH mass. However, all the sources except SDSS J122222.55+041315.7 in Table 1 have BH masses $<10^8 M_\odot$. We investigate the relationship between projected size of the radio jet (D_{proj}) with M_{BH} and radio power at 1.4 GHz ($P_{1.4}$) for NLSy1 galaxies in Figure 4. The red point in each panel represents SDSS J103024.95+551622.7. The magenta polygons represent NLSy1 galaxies that have larger than 20 kpc extended radio structures (see Table 1). No correlation is found between the projected size with M_{BH} (or jet power). When the sources are put in the *WISE* W1-band absolute magnitude versus radio power diagram, a strong correlation is found. The points in this plot are the NLSy1 galaxies from Rakshit et al. (2017) which are detected in FIRST and *WISE* in the W1-band with signal-to-noise ratio >10 . The Spearman correlation test on the full sample yields a correlation coefficient (r) of -0.6 and a very low p -value ($p < 1 \times 10^{-20}$), suggesting a significant negative correlation where absolute IR magnitude decreases with radio power. The BH mass of all those objects is plotted against their radio power in the right panel. We found a positive correlation having $r = 0.4$ which is similar to that found by Liu et al. (2006) between jet power and BH mass, suggesting high-powered jets originate from massive AGNs. From Figure 4 (bottom right panel) it is evident that NLSy1 galaxies with >20 kpc radio structure predominantly occupy the region with large radio power and high BH mass. In terms

of the projected radio size, SDSS J103024.95+551622.7 is the second-largest NLSy1 galaxy after SDSS J110006.07+442144.3.⁹ In Figure 4, it follows the $W1 - P_{1.4}$ anti-correlation and $M_{\text{BH}} - P_{1.4}$ correlation, like other kpc scale radio-emitting NLSy1 galaxies.

4.2. A Standard Powerful Radio Galaxy

From the radio spectrum in Figure 1, we see that the spectrum is steep. Considering the lobes of radio galaxies which are optically thin, the derived spectral index of -0.65 ± 0.04 is very close to the theoretical value of injection spectral index¹⁰ of around -0.62 (Kirk et al. 2000; Konar et al. 2013). If the radio jets have the same spectral index of -0.65 then the inverse Compton effect of the cosmic microwave background (CMB) and radio photons together can give rise to an X-ray power-law spectrum in the 0.1 to 10 keV range whose photon index is supposed to be $-(1+0.65) = -1.65$ (Konar et al. 2009). However, for the source SDSS J103024.95+551622.7 the photon index estimated from *ROSAT* data is -2.61 , which is much steeper. To resolve this inconsistency, we need further observations in the 0.1–10 keV band. The presence of a strong [O III] doublet, as seen in Figure 3, indicates strong blackbody emission from the accretion disk, suggesting a standard accretion disk through which the matter is being accreted onto the BH of this source. Therefore, this NLSy1 radio galaxy is a high-excitation radio galaxy in which cold mode accretion is taking place (Allen et al. 2006). Assuming the radio spectral index (-0.65) of this radio galaxy to be the injection spectral index (α_{inj}), the correlation between α_{inj} and jet power Q_{jet} , as published by Konar & Hardcastle (2013) in their Figure 2, we estimated a jet power of this source to be $3 \times 10^{44} \text{ erg s}^{-1}$. This suggests that this NLSy1 galaxy has a jet power typical of classical radio galaxies.

In the lower left panel of Figure 4, we see that there is a strong correlation between $W1$ and $P_{1.4}$. Most of the luminosity in the W1-band of *WISE* comes from the old stars in the bulge. This means the greater the $W1$ luminosity, the heavier the bulge, and the heavier the BH mass (Kormendy & Richstone 1995). With a heavier BH mass, we might get higher jet power provided the Eddington-scaled mass accretion rate and the spin of the BHs are in a narrow range. We indeed get a correlation between BH mass and the radio power at 1.4 GHz (which is a proxy of jet power). Therefore, we can expect that all NLSy1 galaxies are accreting with Eddington-scaled mass accretion rate within a very narrow range. If spin of the BH has a role in determining the jet power, then all NLSy1 galaxies must have spin within a very narrow range (or jet power has no dependence on the spin). Therefore, the correlations in the left and right bottom panels are as expected.

Similarly, the absence of correlation in the top right and top left panels are as expected. Let us consider the top left panel, where source size versus M_{BH} is plotted. If the source size depended only on the jet power, then we would perhaps obtain a correlation between source size and BH mass. However, the source size depends on jet power (Q_{jet}), density (ρ_{amb}) of the ambient medium, and the angle (θ) of the jet with the line of sight. Even if the jet power is correlated with BH mass, the scatter of the values of ρ_{amb} and θ from source to source will

⁹ Note that SDSS J110006.07+442144.3 does not satisfy the [O III]/ $H\beta$ flux ratio <3 (Tanaka et al. 2014) required for NLSy1 galaxy classification.

¹⁰ A negative sign is used to match the definition of spectral index.

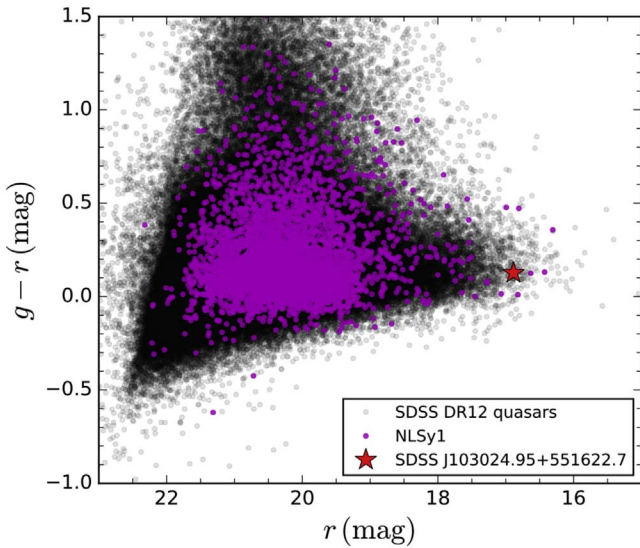


Figure 5. Optical $g - r$ color vs. r magnitude diagram, showing NLSy1 galaxies (magenta dots), SDSS quasars (black dots), and SDSS J103024.95+551622.7 (star).

spoil any correlation between source size and BH mass. Since BH mass and $P_{1.4}$ are correlated, we do not expect to get any correlation between source size and $P_{1.4}$, as there is no correlation between source size and BH mass. A larger sample will help to address this.

4.3. Link With Specra

NLSy1 galaxies are more often associated with spiral or disk galaxies with rich gaseous central regions (Deo et al. 2006; Ohta et al. 2007). Not only in NLSy1 galaxies but also in general Seyfert galaxies, radio-loud galaxies with over 100 kpc large radio lobes are rare. While almost all large (over 100 kpc) radio galaxies are hosted in elliptical galaxies, only six of them are known to be hosted in disk/spiral galaxies with large radio lobes. In Figure 5, we plot the optical $g - r$ color against r magnitude of NLSy1 galaxies from Rakshit et al. (2017) in dots (magenta) along with SDSS quasars in the background (black). Our target is represented by a star symbol having a $g - r$ color of 0.10 mag. According to Banerji et al. (2010), a galaxy can be defined as a spiral if the observer-frame $g - r < 0.6$ mag (see also Tempel et al. 2011). Thus, SDSS J103024.95+551622.7 can be considered as a spiral galaxy following the above criteria. According to the plot, the majority of NLSy1 galaxies are expected to be spiral. However, deep imaging observations of NLSy1 galaxies are needed to confirm if their hosts are indeed spirals. Nevertheless, a few examples of spiral host radio galaxies are known, such as J0313-192 (Ledlow et al. 1998), Specra (Hota et al. 2011), J0314-1906, J2345-0449, J0836+0532, and MCG+07-47-10 (Hota et al. 2016). It is likely that such spiral host radio galaxies could be more frequent in the early universe, prior to the quasar/radio galaxy era ($z \sim 2-3$) and when spiral galaxies were more prevalent than the merger-remnant ellipticals (Hota et al. 2016). Thus, this new object reported here, SDSS J103024.95+551622.7, hosted in a spiral galaxy, may represent an opportunity to investigate non-standard modes of relativistic jet production in passively evolving galaxies with smaller BH masses which

may have been more common in the early universe, prior to the rise of merger-remnant ellipticals and supermassive BHs.

4.4. Doppler Factor, Inclination Angle, and Age

The observed core dominance parameter (r_{obs} ; Orr & Browne 1982) can be calculated from the ratio of core (S_{core}) to lobe (S_{lobe}) flux densities. At 1.4 GHz from FIRST, the source has an integrated core flux density of 32.7 mJy with the SW and NE lobes having integrated flux densities of 21.9 mJy and 95.3 mJy respectively. The observed core dominance parameter is thus $r_{\text{obs}} = 0.28$. This value is higher than that known for radio galaxies with FR I and FR II radio morphologies having median values $r_{\text{obs}} = 0.022$ and 0.003 respectively (Morganti et al. 1997). We note that blazars show extreme core dominance, which is caused by Doppler boosting (Chen et al. 2015). We calculate the Doppler factor (δ) following Doi et al. (2012)

$$\delta_{\text{core}}^{(3-\alpha)} = \frac{r_{\text{obs}}}{r_{\text{int}}}, \quad (1)$$

where r_{int} is the intrinsic core dominance parameter and α is the core spectral index. We assumed the core spectral index to be flat with $\alpha = 0$. The calculation of r_{int} needs an estimation of the intrinsic core power. We derived the intrinsic core power using the empirical relation known for radio galaxies and given by $\log P_c = (0.62 \pm 0.04) \times \log P_t + (7.6 \pm 1.1)$ (Giovannini et al. 2001), where P_c is the core radio power at 5 GHz and P_t is the total radio power at 408 MHz. Using the core flux at 5 GHz and the total flux at 365 MHz from NED, we found $r_{\text{int}} = 0.008$. This is much lower than r_{obs} , suggesting strong Doppler boosting in the core. Using Equation (1) we estimated $\delta = 3.3$.

To constrain the jet speed ($\beta_{\text{core}} = v_{\text{core}}/c$) and inclination angle (θ_{core}) we used the relation $\delta_{\text{core}} = \sqrt{(1 - \beta_{\text{core}}^2) / (1 - \beta_{\text{core}} \cos \theta_{\text{core}})}$. This relation is highly degenerate; however, we obtained values of $\beta_{\text{core}} > 0.87$ and $\theta_{\text{core}} < 12^\circ$. These values are similar to those obtained by Doi et al. (2012) for a sample of NLSy1 galaxies, suggesting that radio-loud NLSy1 galaxies are viewed pole-on. Similar low-inclination values in the range of $10^\circ-15^\circ$ were also obtained by Richards & Lister (2015) for other kpc scale jetted NLSy1 galaxies. Considering a viewing angle of 12° , we found the deprojected size of the source to be $D_{\text{de-proj}} > 116 / \sin 12^\circ > 557$ kpc.

The source exhibits a two-sided structure at kpc scales as seen in Figure 1. Therefore, the flux ratio of the approaching and receding lobes (R_F) were used to calculate the speed of the kpc scale lobes following Richards & Lister (2015)

$$R_F = \left[\frac{(1 + \beta_{\text{kpc}} \cos \theta)}{(1 - \beta_{\text{kpc}} \cos \theta)} \right]^{3-\alpha}, \quad (2)$$

where the spectral index $\alpha = -0.65$. Using $R_F = 4.35$, we obtained $\beta_{\text{kpc}} \cos \theta = 0.2$. Assuming the inclination angle to remain constant between the core and kpc scale lobes, i.e., $\theta = 12^\circ$, we obtained $\beta_{\text{kpc}} \sim 0.2$. Considering the expansion speed of β_{kpc} and a two-sided expansion, we estimated the kinetic age of the source using $t_{\text{kinetic}} = D_{\text{de-proj}} / 2\beta_{\text{kpc}}c$, where $D_{\text{de-proj}}$ is the deprojected size of the source. We obtained $t_{\text{kinetic}} > 4 \times 10^6$ yr.

We also estimated the limiting radiative age of this radio source as $\tau_{\text{rad}} = 50.3 \frac{B^{1/2}}{B^2 + B_{\text{IC}}^2} \frac{1}{\nu_{\text{br}} \sqrt{1+z}}$, where B is the lobe magnetic field expressed in nT, $B_{\text{IC}} = 0.318(1+z)^2$ nT is the CMB equivalent magnetic field (Konar et al. 2006) and ν_{br} is the break frequency (in GHz) observed in the radio spectrum. From the above expression, we get the highest radiative age, when $B = \frac{B_{\text{IC}}}{\sqrt{3}}$. Using $B = \frac{B_{\text{IC}}}{\sqrt{3}} = 0.378$ nT, we obtained a radiative age of 20.2 Myr for the break frequency of 5 GHz. Since there is no break observed in the radio spectrum, the highest observed radio frequency is the lower limit of the break frequency. Thus, $\nu_{\text{br}} > 5$ GHz, corresponds to $\tau_{\text{rad}} < 20.2$ Myr. Both the kinetic and radiative age measurements agree well and provide a strong constraint on the age of SDSS J103024.95+551622.7 to be $>10^6$ yr. This also lies within the age range of 10^5 – 10^7 yr found for other radio-loud NLSy1 galaxies by Doi et al. (2012) and Richards & Lister (2015). It is thus likely that NLSy1 galaxies are young AGNs (Mathur et al. 2001).

5. Conclusion

The object SDSS J103024.95+551622.7 has recently been classified as an NLSy1 galaxy by Rakshit et al. (2017) after carefully modeling the spectrum from the SDSS DR 12 database. From 1.4 GHz radio images obtained by the FIRST survey, the source is found to have a 116 kpc (projected size) large double-lobe FR II-like radio structure and a central core coinciding with the NLSy1 optical galaxy. The core and diffuse emission, associated with the back flow from lobes, conclusively proves the radio lobe and host galaxy association.

The source exhibits a steep radio spectrum with $\alpha = -0.65 \pm 0.04$ estimated from the multi-frequency radio data collected from the NED database. The source is non-variable in the optical and mid-IR bands. We modeled the emission spectra of the source obtained by the SDSS during its two epochs of observation and found that a Lorentzian function best represents the broad component of the $H\beta$ line rather than a Gaussian function. The results obtained from the fitting of two spectra are consistent, having width less than 2200 km s^{-1} and $F([\text{O III}])/F(H\beta) \sim 0.2$, making the source an NLSy1 galaxy as also cataloged by Rakshit et al. (2017). Though nearly a dozen NLSy1 galaxies have been found to have 20–150 kpc extended radio emission, none of them are observed to be fully blown double-lobed, larger than 100 kpc sources as compared to classical radio galaxies. This is a large (116 kpc) FR II-like double-lobe radio source associated with an NLSy1 as the host galaxy. As radio galaxies are typically hosted in ellipticals and extremely rarely (only six) with spirals, understanding of the host or parent population of these NLSy1 galaxies with jets and lobes is far from clear. Radio jets are typically produced in massive spinning BHs with low accretion rate and hence this counter-trend NLSy1 galaxy, SDSS J103024.95+551622.7, with larger than 100 kpc radio lobes, may help to understand the unexplored parameter space of jet production mechanisms and AGN feedback-driven galaxy evolution.

We thank the anonymous referee for his/her critical comments that helped to improve the manuscript. S.R. acknowledges the support by the Basic Science Research Program through the National Research Foundation of Korea government (2016R1A2B3011457). S.R. thanks Neha Sharma (KHU, South Korea) for carefully reading the manuscript.

ORCID iDs

Suvendu Rakshit  <https://orcid.org/0000-0002-8377-9667>

References

- Abdo, A. A., Ackermann, M., Ajello, M., et al. 2009, *ApJ*, 699, 976
 Ai, Y. L., Yuan, W., Zhou, H. Y., et al. 2010, *ApJL*, 716, L31
 Alam, S., Albareti, F. D., Allende Prieto, C., et al. 2015, *ApJS*, 219, 12
 Allen, S. W., Dunn, R. J. H., Fabian, A. C., Taylor, G. B., & Reynolds, C. S. 2006, *MNRAS*, 372, 21
 Antón, S., Browne, I. W. A., & Marchã, M. J. 2008, *A&A*, 490, 583
 Baldi, R. D., Capetti, A., Robinson, A., Laor, A., & Behar, E. 2016, *MNRAS*, 458, L69
 Banerji, M., Lahav, O., Lintott, C. J., et al. 2010, *MNRAS*, 406, 342
 Berton, M., Congiu, E., Järvelä, E., et al. 2018, arXiv:1801.03519
 Boller, T., Brandt, W. N., & Fink, H. 1996, *A&A*, 305, 53
 Boller, T., Freyberg, M. J., Trümper, J., et al. 2016, *A&A*, 588, A103
 Boroson, T. A., & Green, R. F. 1992, *ApJS*, 80, 109
 Calderone, G., Ghisellini, G., Colpi, M., & Dotti, M. 2013, *MNRAS*, 431, 210
 Chen, Y. Y., Zhang, X., Zhang, H. J., & Yu, X. L. 2015, *MNRAS*, 451, 4193
 Congiu, E., Berton, M., Giroletti, M., et al. 2017, *A&A*, 603, A32
 D’Ammando, F., Orienti, M., Doi, A., et al. 2013, *MNRAS*, 433, 952
 D’Ammando, F., Orienti, M., Larsson, J., & Giroletti, M. 2015, *MNRAS*, 452, 520
 Deo, R. P., Crenshaw, D. M., & Kraemer, S. B. 2006, *AJ*, 132, 321
 Doi, A., Nagira, H., Kawakatu, N., et al. 2012, *ApJ*, 760, 41
 Doi, A., Wajima, K., Hagiwara, Y., & Inoue, M. 2015, *ApJL*, 798, L30
 Drake, A. J., Djorgovski, S. G., Mahabal, A., et al. 2009, *ApJ*, 696, 870
 Fanaroff, B. L., & Riley, J. M. 1974, *MNRAS*, 167, 31P
 Gabányi, K. É., Frey, S., Paragi, Z., et al. 2018, *MNRAS*, 473, 1554
 Giovannini, G., Cotton, W. D., Feretti, L., Lara, L., & Venturi, T. 2001, *ApJ*, 552, 508
 Gliozzi, M., Papadakis, I. E., Grupe, D., et al. 2010, *ApJ*, 717, 1243
 Goodrich, R. W. 1989, *ApJ*, 342, 224
 Gu, M., Chen, Y., Komossa, S., et al. 2015, *ApJS*, 221, 3
 Hota, A., Konar, C., Stalin, C. S., et al. 2016, *JApA*, 37, 41
 Hota, A., Sirothia, S. K., Ohya, Y., et al. 2011, *MNRAS*, 417, L36
 Ivezić, Ž., Menou, K., Knapp, G. R., et al. 2002, *AJ*, 124, 2364
 Kapahi, V. K. 1989, *AJ*, 97, 1
 Kellermann, K. I., Sramek, R., Schmidt, M., Shaffer, D. B., & Green, R. 1989, *AJ*, 98, 1195
 Kimball, A. E., & Ivezić, Ž. 2008, *AJ*, 136, 684
 Kirk, J. G., Guthmann, A. W., Gallant, Y. A., & Achterberg, A. 2000, *ApJ*, 542, 235
 Komossa, S., Voges, W., Xu, D., et al. 2006, *AJ*, 132, 531
 Konar, C., & Hardcastle, M. J. 2013, *MNRAS*, 436, 1595
 Konar, C., Hardcastle, M. J., Croston, J. H., & Saikia, D. J. 2009, *MNRAS*, 400, 480
 Konar, C., Hardcastle, M. J., Jamrozy, M., & Croston, J. H. 2013, *MNRAS*, 430, 2137
 Konar, C., Saikia, D. J., Jamrozy, M., & Machalski, J. 2006, *MNRAS*, 372, 693
 Kormendy, J., & Richstone, D. 1995, *ARA&A*, 33, 581
 Lähteenmäki, A., Järvelä, E., Hovatta, T., et al. 2017, *A&A*, 603, A100
 Laor, A. 2000, *ApJL*, 543, L111
 Ledlow, M. J., Owen, F. N., & Keel, W. C. 1998, *ApJ*, 495, 227
 Leighly, K. M. 1999, *ApJS*, 125, 317
 Liu, X., Yang, P., Supriyanto, R., & Zhang, Z. 2016, *IJAA*, 6, 166
 Liu, Y., Jiang, D. R., & Gu, M. F. 2006, *ApJ*, 637, 669
 Mathur, S., Kurazkiewicz, J., & Czerny, B. 2001, *NewA*, 6, 321
 Morganti, R., Oosterloo, T. A., Reynolds, J. E., Tadhunter, C. N., & Migenes, V. 1997, *MNRAS*, 284, 541
 Netzer, H., & Trakhtenbrot, B. 2007, *ApJ*, 654, 754
 Ohta, K., Aoki, K., Kawaguchi, T., & Kiuchi, G. 2007, *ApJS*, 169, 1
 Orr, M. J. L., & Browne, I. W. A. 1982, *MNRAS*, 200, 1067
 Osterbrock, D. E., & Pogge, R. W. 1985, *ApJ*, 297, 166
 Paliya, V. S., Ajello, M., Rakshit, S., et al. 2018, *ApJL*, 853, L2
 Rakshit, S., & Stalin, C. S. 2017, *ApJ*, 842, 96
 Rakshit, S., Stalin, C. S., Chand, H., & Zhang, X.-G. 2017, *ApJS*, 229, 39
 Rani, P., Stalin, C. S., & Rakshit, S. 2017, *MNRAS*, 466, 3309
 Richards, J. L., & Lister, M. L. 2015, *ApJL*, 800, L8
 Sesar, B., Ivezić, Ž., Lupton, R. H., et al. 2007, *AJ*, 134, 2236
 Singal, A. K. 1993, *MNRAS*, 263, 139
 Singh, V., Ishwara-Chandra, C. H., Wadadekar, Y., Beelen, A., & Kharb, P. 2015, *MNRAS*, 446, 599

- Sulentic, J. W., Zwitter, T., Marziani, P., & Dultzin-Hacyan, D. 2000, [ApJL](#), **536**, L5
- Tanaka, M., Morokuma, T., Itoh, R., et al. 2014, [ApJL](#), **793**, L26
- Tempel, E., Saar, E., Liivamägi, L. J., et al. 2011, [A&A](#), **529**, A53
- Véron-Cetty, M.-P., Véron, P., & Gonçalves, A. C. 2001, [A&A](#), **372**, 730
- Wang, T., Brinkmann, W., & Bergeron, J. 1996, [A&A](#), **309**, 81
- Whalen, D. J., Laurent-Muehleisen, S. A., Moran, E. C., & Becker, R. H. 2006, [AJ](#), **131**, 1948
- Wright, E. L., Eisenhardt, P. R. M., Mainzer, A. K., et al. 2010, [AJ](#), **140**, 1868
- Yao, S., Yuan, W., Zhou, H., et al. 2015, [MNRAS](#), **454**, L16
- Yuan, W., Zhou, H. Y., Komossa, S., et al. 2008, [ApJ](#), **685**, 801
- Zhou, H., Wang, T., Yuan, W., et al. 2006, [ApJS](#), **166**, 128